



Mapping of geochemical anomalies in the Zagros ophiolites stream sediments by fractal and classical analyses: implication for mineral exploration in Iraqi Kurdistan

Mohammad Pirouei^{1,2} · Kamal Kolo¹ · Stavros P. Kalaitzidis³ · Jamshid Sobhanverdy⁴

Received: 7 November 2021 / Accepted: 23 February 2022 / Published online: 14 March 2022
© Saudi Society for Geosciences 2022

Abstract

Several mineralizations of chromitites, iron-rich gossanite and sulphides occur in the Rayat area of Zagros suture-ophiolites nappe in NE Iraqi Kurdistan. Nevertheless, no systematic geochemical mapping has been carried out in the region. This study brings forth the results of an extensive geochemical survey along with geochemical anomalies in the area that will warrant subsequent mineral exploration. In this work, 41 samples were collected from the stream network of the Rayat area, and analyzed for their chemical elements concentration content, focusing on the distribution patterns mainly of Ba, Co, Cr, Cu, Ni, Pb, V, and Zn. Concentration-area (C-A) fractal analysis, median absolute deviation (MAD), and Tukey's inner fence (TIF) statistical analysis methods were concurrently applied for the detection of geochemical anomalies and their differentiation from existing background levels in the area. The resulting thresholds practically produced identical maps of the geochemical anomalies, pointing out to a reliable outcome. We report here that the obtained results delineate three promising areas with high potential mineralization anomalies of Cu, Ni, Zn, and Cr in the south and southeast part of the Rayat area. These anomalies indicate new prospects for unexplored ore minerals in the area.

Keywords Geochemical mapping · Anomalies · Fractal method · MAD · TIF · Zagros · Iraqi Kurdistan

Introduction

Stream sediments have been broadly utilized for geochemical exploration aims. The elemental composition of stream sediments delivers valuable information on potential mineralizations (Rantitsch 2000), particularly in the initial phases of searching for hidden mineral deposits (Yousefi et al. 2014). One key factor for the accurate interpretation of stream sediment geochemistry

is to separate the targeted elements concentration and distribution patterns from the local background levels in each stream, in order to eliminate factors not related to mineralization (Carranza 2004). By doing so, the residual values will correspond more accurately to the effects of irregular geological processes such as mineralization processes (Carranza and Hale 1997). Classical statistical methods employing probability plots (Sinclair 1991) have been widely used for separating the background from the measured anomalies. By using these methods, the thresholds are determined by the average value and the standard deviation of the data (Li et al. 2003), while only the frequency distribution of elemental concentrations is used for separating the anomaly from the background. However, since they do not take into account the data spatial distribution, valuable information can be omitted (Parsa et al. 2016). Median + 2MAD remains a reliable classical method that is much stronger against the influence of data outliers that are prevalent in geochemical data sets (Reimann et al. 2005). This method provides very low threshold values, meaning it yields many sites for further investigation.

Responsible Editor: Domenico M. Doronzo

✉ Mohammad Pirouei
mohammad.askandar@soran.edu.iq

¹ Scientific Research Center, Soran University, PO Box 624, Soran, KRG, Iraq

² Department of Petroleum Geosciences, Faculty of Sciences, Soran University, PO Box 624, Soran, KRG, Iraq

³ Section of Earth Materials, Department of Geology, University of Patras, 265 04 Patras, Greece

⁴ Department of Geology, Faculty of Natural Resources, University of Kharazmi, Tehran, Iran

Tukey (1977) on the other hand had introduced the paradigm of exploratory data analysis (EDA) to analyze and interpret univariate data that do not show a normal distribution. EDA includes the collection of descriptive statistical and, mostly, graphical tools designed to (1) gain maximum intuition into a data set, (2) discover data structure, (3) define important variables in the data, (4) find outliers and anomalies, (5) propose and test hypotheses, (6) develop careful models, and (7) distinguish best possible treatment and interpretation of data. The descriptive statistical and graphical tools used in EDA are based on the data itself, not the data distribution model (e.g. normal distribution). The boxplot, density trace, and jittered one-dimensional scatterplot are the main graphical tools used in uni-element geochemical data analysis (Kürzl 1988; Reimann et al. 2005; Reimann and de Caritat 2017). A combination of graphics can indicate any 'anomalies' in an univariate data set. In recent years, fractal methods such as concentration - area (C-A) have been suggested and applied in the published literature on the segregation of geochemical anomalies from the background (Cheng 1999; Cheng et al. 2000).

Several fractal methods have been applied for separation anomalies from background, such as concentration-area (C-A) (Cheng 1999), concentration dimension (C-D) (Changjiang et al. 2003), and concentration number (C-N) (Mao et al. 2004). In this methods, the influence of a stream sediment sampling point covers only the upstream area of the catchment and not the downstream area, which in turn will be influenced by the next sampling point downstream (Spadoni 2006; Bai et al. 2010; Daya and Afzal 2015; Parsa et al. 2016; Ghezlbash and Maghsoudi 2018). Stream sediments genetically are considered as a mixture of natural grains produced by weathering and erosion processes, as well as anthropogenic particles of different nature transported into catchment basins (Spadoni 2006). Therefore, the geochemical features of each sample can be regarded as a mixture of geological sediments and material of anthropogenic sources that are transported along with the hydrographical network (Bölviken et al. 1986).

The goal of this research is the identification of geochemical anomalies in the Rayat area, lying on the Kurdistan ophiolitic terrain, in order to locate potential mineralizations. Recently, the hydrothermal formation of listvenite and gossanite in the studied area has been reported (Pirouei et al. 2020, 2021), and along with the vast occurrence of ophiolitic bedrock, favourable prospects for mineral exploration are expected. The explored area is a treacherous mountainous terrain with uncleared landmines field remnants of the Iraq-Iran conflict in the

1980s of the last century. Consequently, geochemical exploration and geological studies of the area are scarce. This study is the first systematic geochemical exploration in the region. In this paper, parametric and fractal methods are applied to map the spatial distribution patterns of Ba, Co, Cr, Cu, Ni, Pb, V, and Zn anomalies in the studied area.

Geological setting

The Rayat area is located between longitude ($44^{\circ} 54.00' E$ – $45^{\circ} 04.00' E$) and latitude ($36^{\circ} 37.00' N$ – $36^{\circ} 44.00' N$) covering around 120 km². Tectonically, it is a portion of the Iraqi Zagros Suture Zone (IZSZ) (Fig. 1a). The outcropping lithostratigraphic units of Paleocene–Upper Eocene in the area belong to the Walsh Group that comprises (1) the lower Calcareous Shale Group of late Eocene–Paleocene age, (2) the middle Volcano-Sedimentary Group, consisting of basalts and spilites, as well as breccia and conglomerates of volcano-sedimentary origin, and (3) the upper Calcareous-Argillite Group consisting of calcareous argillites, limestone, ferruginous conglomerates, jasper rocks, and Fe-rich sandstones (Vasiliev and Pentelikov 1962).

The intrusive rocks of the Rayat area include peridotites (dunite and harzburgite) and gabbro formed as sheets and sills. The majority of primary mafic to ultramafic intrusive rocks were altered to serpentinites that sporadically host chromite lenses. The encountered serpentinites are part of the ophiolitic mélangé that occurs predominantly along with thrust faults, which juxtapose the Qulqula Radiolarite with the Walsh Volcano-Sedimentary Group (Aswad et al. 2011). The serpentinites were later on subjected to hydrothermal alteration by solutions rich in K, Si, Ca, leading to the formation of listvenites; the circulation of the hydrothermal fluids was controlled by tectonic structures (Fig. 2) (Pirouei et al. 2020).

Material and methods

Fieldwork

The sample collection and preparation protocols followed the guidelines in Lech et al. (2007). Figure 3 shows the specific location of the samples on the related catchment areas. The study area is considerably rugged and inaccessible mountainous terrain compounded by the presence of uncleared minefields remaining from the previous war in

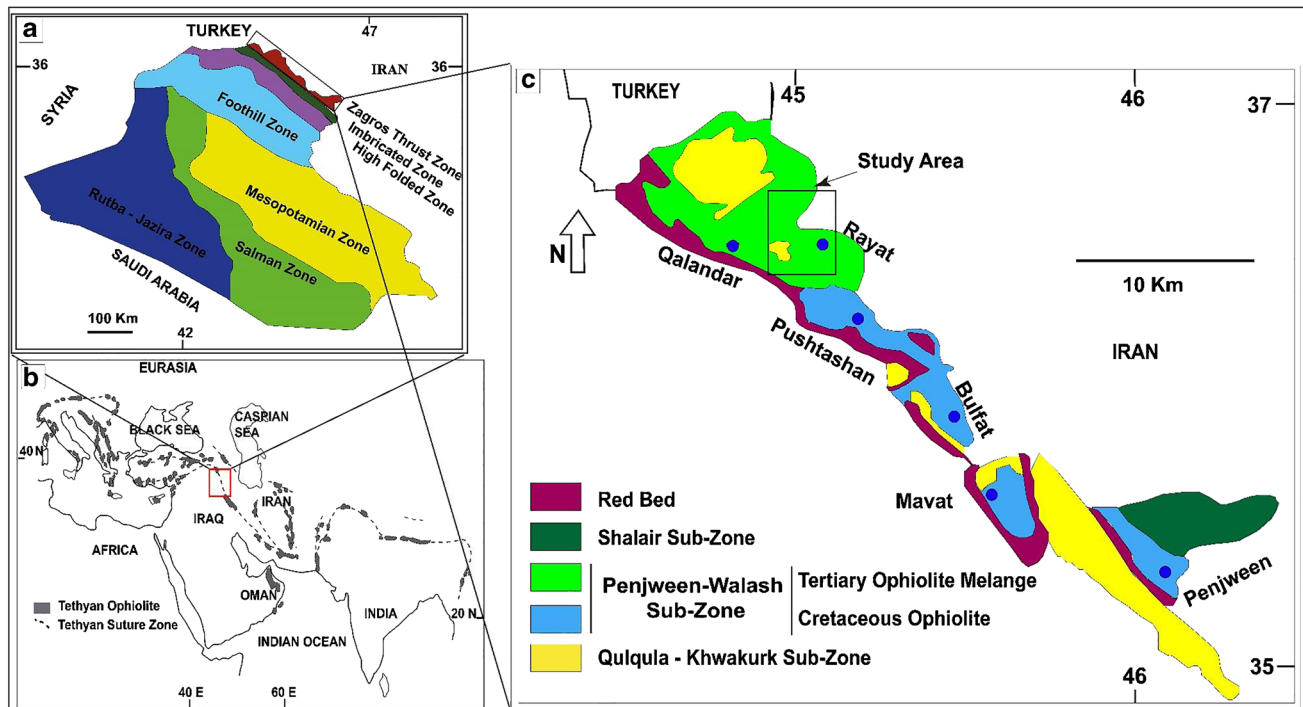


Fig. 1 a–c General geological map of the Iraqi Zagros Suture Zone including the study area (after Moores et al., 2000 and Sissakian, 2000)

the area. Under these field restrictions, only the accessible sites were sampled.

Forty-one samples typically consisting of silts and fine sands were collected from active and seasonal streams. The selected samples were sieved, and the < 80 mesh part was retained in thick polyethylene bags, and later dried in the lab at room temperature for 72 h and ground to -0.125 mm in preparation for X-ray fluorescence (XRF) analysis. The analysis was duplicated for every eighth sample for data quality control. Moreover, the precision of the instrument was calculated by the method of Thompson and Howarth (1976) on duplicate samples; the results showed around 10% precision.

Statistical evaluation—separation of anomalies from background

The statistical analysis was performed with SPSS 24 software. In order to replace censored data, the simple substitution method was employed.

In this study, three methods were conducted to separate the anomalies from the background: (i) $M+2MAD$ method (Reimann et al. 2005), (ii) exploratory data analysis (EDA) method and TIF (Tukey 1977), and (iii) C-A fractal method of (Cheng et al. 1994).

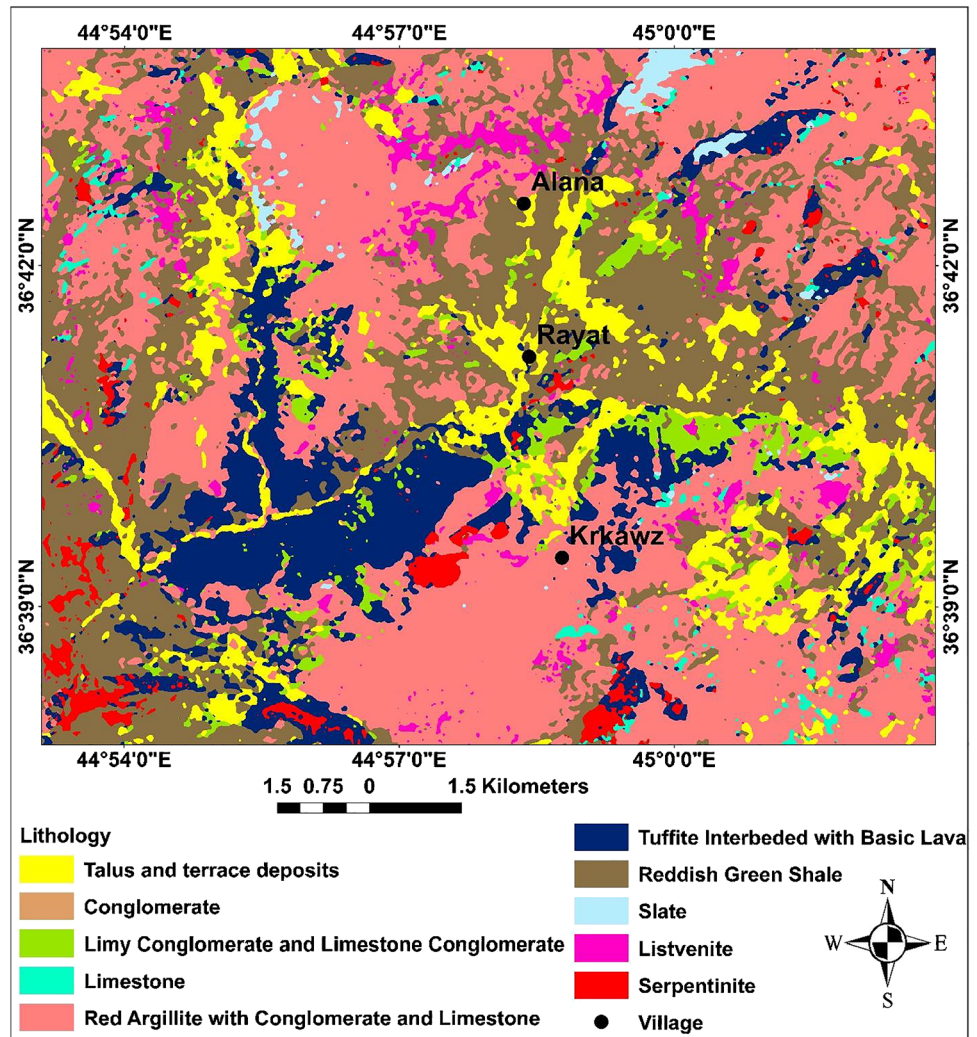
Median + 2MAD

This method has been proposed by Reimann et al. (2005) instead of Mean + 2STD. The reduced sensitivity of this method towards the influence of data outliers made it widely used in threshold estimation (Reimann et al. 2005; Zheng et al. 2014). The MAD delivers a value that should be multiplied by a constant (for normal distribution 1.4826) so that it adapts to the underlying distribution, to give the Median + 2MAD (Reimann et al. 2008, 2018). In environmental geochemical surveys, the method provides excellent results (Mrvić et al. 2010), while additionally, the method is getting popular in exploration geochemistry (Chen et al. 2016; Reimann and de Caritat 2017).

Tukey's inner fences (TIF)

This method was proposed by Tukey (1977) for univariate data analysis and interpretation. It uses density trace, jittered one-dimensional scatterplot, and boxplot as main graphical tools (Kürzl 1988; Reimann et al. 2005; Reimann and de Caritat 2017). In this method, a box plot will be drawn for the data. The boxplot defines 5-number summary statistics named minimum, the lower hinge (LH), median, the upper hinge (UH), and maximum. The parameters of the boxplot

Fig. 2 Geological map of the Rayat area (updated from Vasiliev and Pentelikov 1962 and Pirouei et al. 2020)



are interquartile range (IQR) or hinge width (HW), lower inner fence (LIF), lower outer fence (LOF), upper inner fence (UIF), upper outer fence (UOF), lower whisker (LW), and upper whisker (UW) (Tukey 1977; Hoaglin et al. 2000). Because the box represents approximately 50% of a univariate data set, therefore at most 25% of data can be outliers, but these values do not significantly affect the median and the hinges. The boxplot is resistant and robust against extreme outliers in univariate data because the IQR or the hinge width defines the inner fences; outliers do not seriously affect them.

According to a boxplot uni-element, the geochemical data set usually is divided into five classes (1) minimum–LW considered extremely low background; (2) LW–LH as low background; (3) LH–UH as background; (4) UH–UW considered high background; and (5) UW–maximum shows the anomalies. UIF and UOF can be considered a threshold for separating anomalies from the background and high anomalies from anomalies,

respectively (e.g. Bounessah and Atkin 2003; Reimann et al. 2005).

Concentration-area fractal model

Cheng et al. (1994) suggested the concentration-area (C-A) fractal model for determining different thresholds (Chen et al. 2016). The equation that expresses this model is (Cheng et al. 1994):

$$A(\rho \leq v) \propto \rho^{-a_1}; A(\rho > v) \propto \rho^{-a_2}$$

In this equation, the occupied area is considered $A(\rho)$ that has concentration amounts larger than contour amounts ρ ; v refers to the threshold value, and a_1 and a_2 are fractal dimensions of an anomaly and background. Cheng et al. (1994) utilized two methods for deriving $A(\rho)$: (1) the calculation of the area surrounded by the contour amount ρ on a geochemical contour map (2) the computation of $A(\rho)$ by counting

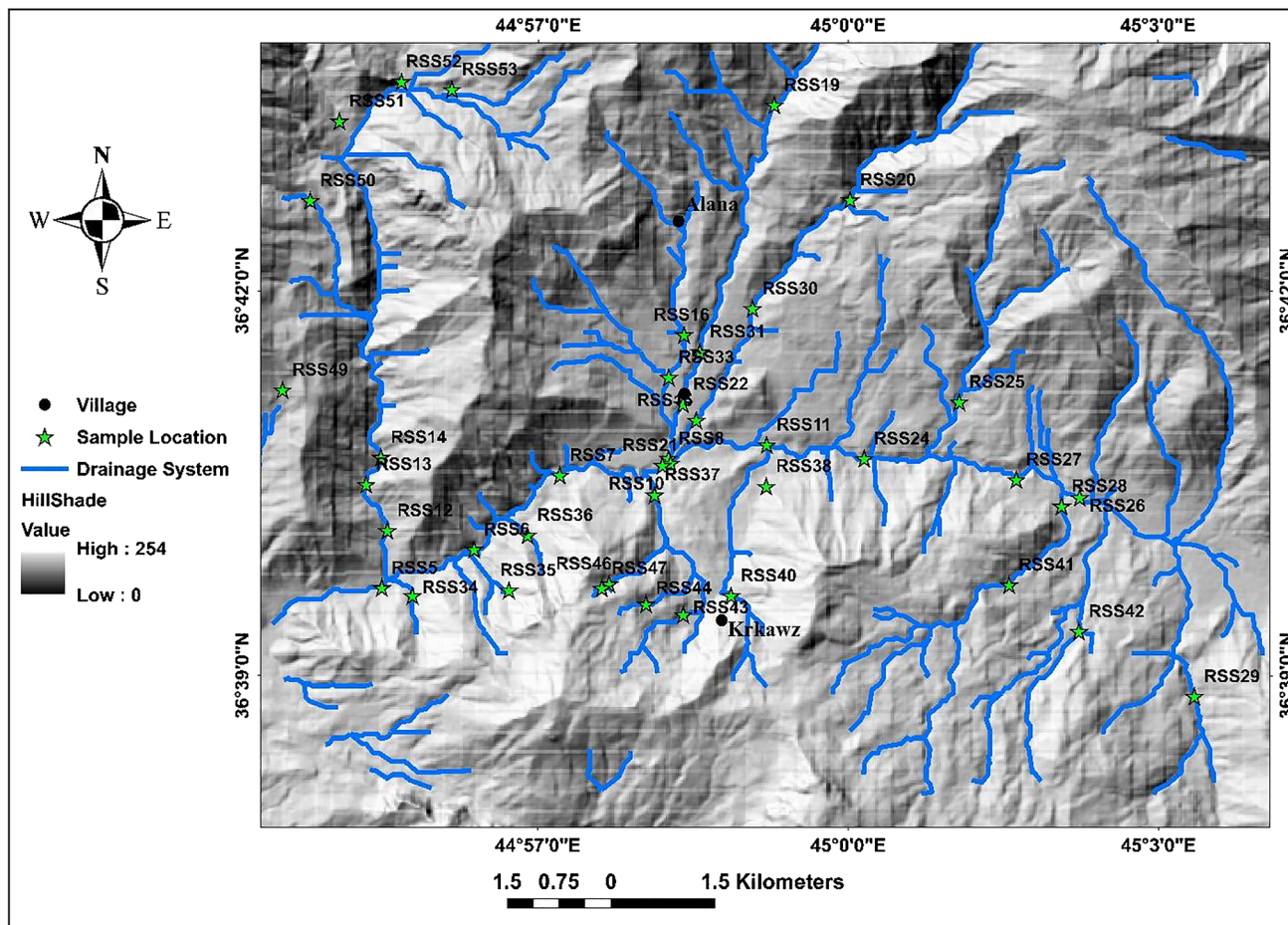


Fig. 3 Sample’s location and drainage system on the hillshade map of the Rayat area

the number of pixels bigger than or equal to v . After that, the breakdowns among straight-line parts on log–log plots and the given amounts of ρ were applied for determining the thresholds.

In order to calculate the C-A for Ba, Co, Cr, Cu, Ni, Pb, V, and Zn elements, it is necessary to convert samples distribution points to raster. The dimensions of raster pixels gave occupied area per each concentration value. Kriging/cokriging and inverse distance weighting were used to data interpolation of sampled points. Produced raster by IDW method for each element shows reasonable results that are close to field observations and geology of the study area. General properties, search neighbourhood, predicted value, and weights have been left as default values by ArcGIS.

Analytical techniques

X-ray fluorescence (XRF) analysis for major and minor elements in stream sediments was performed on pressed powdered samples by a RIGAKU ZSX PRIMUS II spectrometer, equipped with Rh-anode at the Laboratory of

Electron Microscopy and Microanalysis, Faculty of Natural Sciences, University of Patras. The values of loss on ignition (LOI) were measured by burning 1 g at 950 °C for 2 h (Heiri et al. 2001) using a Selecta® muffle furnace. The analysis was conducted at the University of Patras, Greece.

Results

Table 1 shows the XRF results of the stream sediment samples, whereas geochemical maps were produced for the elements Ba, Co, Cr, Cu, Ni, Pb, V, and Zn.

Data processing

Normalization of the data

Geochemical data usually does not show a normal distribution (Reimann and Filzmoser 2000). Most of the

Table 1 XRF Geochemical results of the stream sediment samples from the Rayat area

| CODE | Na ₂ O | MgO | Al ₂ O ₃ | SiO ₂ | P ₂ O ₅ | K ₂ O | CaO | TiO ₂ | MnO | Fe ₂ O ₃ | LOI | S | V | Cr | Co | Ni | Cu | Zn | Rb | Sr | Y | Zr | Nb | Ba | Hf | Pb | La | Ce | Th | |
|-------|-------------------|-------|--------------------------------|------------------|-------------------------------|------------------|-------|------------------|------|--------------------------------|-------|---------|--------|---------|--------|---------|--------|--------|-------|--------|-------|--------|-------|--------|-------|-------|-------|--------|-------|-------|
| % | % | % | % | % | % | % | % | % | % | % | % | mg/kg | mg/kg | mg/kg | mg/kg | mg/kg | mg/kg | mg/kg | mg/kg | mg/kg | mg/kg | mg/kg | mg/kg | mg/kg | mg/kg | mg/kg | mg/kg | mg/kg | mg/kg | mg/kg |
| RSS5 | 2.10 | 11.63 | 8.11 | 48.17 | 0.14 | 1.16 | 10.24 | 0.92 | 0.12 | 11.05 | 8.05 | 484.23 | 208.17 | 2027.46 | 38.38 | 459.06 | 148.02 | 118.76 | 43.48 | 305.23 | 28.63 | 117.90 | 6.40 | 216.67 | < 1 | 11.01 | 43.00 | 62.00 | 3.00 | |
| RSS6 | 1.49 | 12.54 | 7.67 | 49.54 | 0.11 | 1.02 | 10.72 | 0.82 | 0.10 | 9.58 | 9.45 | < 1 | 182.76 | 1160.23 | 7.26 | 594.53 | 136.35 | 85.60 | 44.72 | 248.98 | 28.22 | 89.64 | 6.27 | 144.46 | < 1 | 12.04 | 30.00 | 83.00 | 4.00 | |
| RSS7 | 1.28 | 11.27 | 8.60 | 44.86 | 0.10 | 0.97 | 14.75 | 0.75 | 0.08 | 7.98 | 11.82 | < 1 | 173.77 | 1026.02 | 17.63 | 560.99 | 131.37 | 79.56 | 50.68 | 249.97 | 27.31 | 94.46 | 6.67 | 142.76 | < 1 | 12.04 | 24.00 | 85.00 | 5.00 | |
| RSS8 | 1.82 | 13.92 | 6.84 | 52.87 | 0.08 | 1.13 | 6.55 | 0.80 | 0.10 | 10.63 | 6.90 | < 1 | 180.76 | 1094.09 | < 1 | 605.71 | 135.36 | 91.64 | 50.68 | 160.34 | 27.31 | 87.71 | 3.87 | 109.62 | < 1 | 14.05 | 21.00 | 93.00 | 5.00 | |
| RSS10 | 2.02 | 14.07 | 6.71 | 48.49 | 0.08 | 0.81 | 8.33 | 0.76 | 0.10 | 9.56 | 11.70 | 510.92 | 166.78 | 2046.20 | 60.15 | 787.63 | 173.18 | 100.71 | 39.75 | 214.12 | 17.30 | 87.71 | 3.47 | 135.11 | 14.00 | 13.04 | 17.00 | 90.00 | 3.00 | |
| RSS11 | 1.35 | 13.52 | 7.18 | 47.84 | 0.10 | 0.93 | 9.75 | 0.82 | 0.11 | 10.20 | 9.56 | < 1 | 191.75 | 2340.87 | 22.81 | 828.28 | 169.19 | 94.66 | 40.74 | 208.14 | 26.40 | 113.74 | 3.07 | 138.51 | 2.00 | 12.04 | 27.00 | 83.00 | 5.00 | |
| RSS12 | 1.90 | 8.84 | 9.75 | 51.88 | 0.19 | 1.54 | 9.78 | 0.89 | 0.13 | 8.99 | 9.07 | < 1 | 205.73 | 555.31 | 91.26 | 298.79 | 111.47 | 89.63 | 66.58 | 319.68 | 30.05 | 118.56 | 7.07 | 338.20 | < 1 | 13.04 | 23.00 | 41.00 | 6.00 | |
| RSS13 | 1.99 | 9.63 | 8.69 | 56.57 | 0.16 | 1.51 | 7.32 | 0.99 | 0.13 | 10.56 | 5.08 | < 1 | 254.66 | 949.19 | 62.22 | 297.77 | 110.47 | 83.59 | 49.69 | 330.64 | 38.24 | 125.30 | 6.80 | 318.65 | < 1 | 11.04 | 53.00 | 60.00 | 5.00 | |
| RSS14 | 1.85 | 9.87 | 8.38 | 57.12 | 0.15 | 1.51 | 6.23 | 0.84 | 0.13 | 9.59 | 6.86 | < 1 | 214.71 | 701.19 | 58.07 | 366.88 | 120.43 | 89.63 | 63.60 | 303.75 | 35.51 | 120.48 | 6.27 | 342.45 | < 1 | 13.04 | 31.00 | 53.00 | 6.00 | |
| RSS15 | 1.78 | 14.28 | 6.61 | 54.01 | 0.08 | 1.07 | 5.06 | 0.80 | 0.11 | 10.87 | 6.82 | < 1 | 184.75 | 1237.05 | < 1 | 614.86 | 135.36 | 92.65 | 46.71 | 157.35 | 28.22 | 95.42 | 2.80 | 90.92 | 1.00 | 14.05 | 23.00 | 101.00 | 5.00 | |
| RSS16 | 1.68 | 11.42 | 7.86 | 55.41 | 0.10 | 1.41 | 3.76 | 0.78 | 0.20 | 10.10 | 7.68 | < 1 | 160.79 | 933.63 | 6.22 | 674.82 | 161.23 | 98.69 | 59.63 | 241.01 | 30.05 | 108.92 | 5.20 | 286.36 | < 1 | 18.06 | 38.00 | 56.00 | 6.00 | |
| RSS19 | 1.29 | 12.92 | 6.86 | 45.71 | 0.10 | 0.89 | 9.32 | 0.79 | 0.11 | 9.74 | 9.70 | < 1 | 144.81 | 865.55 | 0.00 | 658.56 | 144.31 | 92.65 | 85.46 | 226.07 | 23.67 | 105.06 | 3.87 | 318.65 | 1.00 | 15.05 | 34.00 | 45.00 | 8.00 | |
| RSS20 | 2.03 | 13.81 | 6.93 | 53.17 | 0.10 | 1.10 | 4.02 | 0.86 | 0.11 | 11.39 | 6.81 | < 1 | 185.75 | 1016.29 | 22.81 | 530.51 | 128.39 | 96.68 | 45.71 | 123.49 | 27.31 | 89.64 | 2.67 | 100.27 | 1.00 | 15.05 | 19.00 | 99.00 | 5.00 | |
| RSS21 | 1.94 | 12.99 | 6.89 | 51.60 | 0.10 | 1.10 | 6.55 | 0.84 | 0.13 | 10.83 | 6.54 | 209.75 | 195.16 | 1340.59 | 44.61 | 548.04 | 157.76 | 88.57 | 41.50 | 232.13 | 34.18 | 90.84 | 7.68 | 144.73 | < 1 | 14.01 | 42.00 | 84.00 | 4.00 | |
| RSS22 | 1.99 | 12.11 | 7.54 | 51.53 | 0.12 | 1.27 | 7.55 | 0.85 | 0.13 | 10.49 | 8.02 | 258.95 | 190.15 | 1058.61 | 40.46 | 490.41 | 151.91 | 86.55 | 48.42 | 269.67 | 31.41 | 99.54 | 7.52 | 167.85 | < 1 | 12.01 | 34.00 | 72.00 | 4.00 | |
| RSS24 | 1.36 | 11.66 | 7.89 | 47.67 | 0.11 | 0.97 | 9.90 | 0.75 | 0.11 | 9.24 | 12.85 | 656.33 | 170.77 | 1465.60 | 42.52 | 695.14 | 155.26 | 93.66 | 48.69 | 206.15 | 21.85 | 106.03 | 3.87 | 156.35 | < 1 | 13.04 | 25.00 | 78.00 | 4.00 | |
| RSS25 | 1.89 | 14.52 | 6.89 | 52.03 | 0.10 | 1.03 | 3.66 | 0.87 | 0.12 | 12.16 | 6.52 | 244.98 | 197.74 | 1420.86 | 43.56 | 586.40 | 138.34 | 94.66 | 42.73 | 93.61 | 30.05 | 83.86 | 3.20 | 123.21 | < 1 | 14.05 | 21.00 | 91.00 | 5.00 | |
| RSS26 | 2.06 | 13.77 | 8.07 | 51.54 | 0.11 | 1.15 | 6.28 | 0.89 | 0.13 | 11.08 | 8.72 | 280.35 | 186.75 | 1258.45 | 43.56 | 558.96 | 142.32 | 98.69 | 46.71 | 231.05 | 27.31 | 102.17 | 4.40 | 177.60 | < 1 | 14.05 | 38.00 | 72.00 | 4.00 | |
| RSS27 | 1.63 | 14.15 | 7.00 | 48.50 | 0.10 | 0.95 | 7.16 | 0.89 | 0.13 | 12.42 | 8.29 | 317.03 | 203.73 | 2301.00 | 53.93 | 727.67 | 162.23 | 97.68 | 37.76 | 229.06 | 30.96 | 108.92 | 4.00 | 136.81 | < 1 | 12.04 | 23.00 | 87.00 | 3.00 | |
| RSS28 | 1.74 | 19.38 | 5.25 | 47.36 | 0.08 | 0.53 | 7.05 | 0.88 | 0.09 | 9.86 | 9.60 | 1879.91 | 188.75 | 5595.92 | 225.03 | 2950.30 | 514.55 | 137.97 | 18.88 | 193.20 | 15.48 | 115.67 | 1.20 | 79.03 | 34.00 | 11.04 | 24.00 | 105.00 | 1.00 | |
| RSS29 | 2.32 | 10.50 | 9.28 | 51.82 | 0.15 | 1.53 | 6.54 | 0.90 | 0.16 | 9.88 | 8.09 | 400.87 | 193.74 | 974.47 | 39.41 | 381.11 | 120.43 | 96.68 | 56.64 | 282.84 | 31.87 | 124.34 | 4.93 | 220.08 | < 1 | 13.04 | 47.00 | 73.00 | 5.00 | |
| RSS30 | 2.19 | 12.00 | 7.93 | 52.03 | 0.12 | 1.28 | 5.47 | 0.89 | 0.14 | 10.46 | 7.49 | 324.89 | 185.75 | 1079.51 | 41.48 | 485.79 | 133.36 | 95.67 | 49.69 | 197.19 | 30.96 | 106.99 | 4.53 | 168.25 | < 1 | 15.05 | 31.00 | 79.00 | 5.00 | |
| RSS31 | 3.29 | 12.12 | 7.56 | 55.56 | 0.09 | 1.10 | 5.19 | 0.81 | 0.09 | 9.84 | 7.10 | 196.51 | 186.75 | 1005.59 | 59.11 | 412.62 | 123.41 | 91.64 | 45.71 | 276.86 | 18.21 | 90.60 | 4.80 | 152.95 | 17.00 | 12.04 | 50.00 | 87.00 | 4.00 | |
| RSS33 | 2.04 | 10.48 | 8.34 | 54.45 | 0.12 | 1.40 | 4.99 | 0.83 | 0.15 | 9.91 | 9.84 | 293.45 | 166.78 | 911.26 | 44.59 | 616.89 | 153.27 | 95.67 | 61.61 | 229.06 | 28.22 | 109.88 | 5.07 | 243.88 | < 1 | 17.06 | 40.00 | 67.00 | 5.00 | |
| RSS34 | 2.85 | 6.13 | 11.48 | 50.48 | 0.27 | 2.56 | 6.67 | 1.09 | 0.33 | 9.90 | 8.64 | 307.86 | 168.78 | 196.45 | 53.93 | 153.46 | 107.49 | 105.74 | 66.58 | 508.91 | 33.69 | 140.73 | 11.20 | 583.77 | < 1 | 21.07 | 58.00 | 75.00 | 4.00 | |
| RSS35 | 2.18 | 9.20 | 9.41 | 50.93 | 0.19 | 1.86 | 7.10 | 0.78 | 0.21 | 9.40 | 11.57 | 398.25 | 138.82 | 758.57 | 54.96 | 612.82 | 163.22 | 105.74 | 71.55 | 428.24 | 24.58 | 123.38 | 8.80 | 492.85 | < 1 | 17.06 | 43.00 | 48.00 | 5.00 | |
| RSS36 | 2.70 | 11.35 | 9.80 | 47.68 | 0.25 | 1.85 | 3.70 | 1.06 | 0.17 | 12.93 | 10.04 | 449.34 | 156.79 | 605.88 | 72.59 | 488.84 | 155.26 | 111.78 | 53.66 | 518.86 | 30.05 | 140.73 | 9.73 | 625.41 | < 1 | 13.04 | 49.00 | 87.00 | 5.00 | |
| RSS37 | 1.67 | 11.70 | 7.60 | 47.64 | 0.17 | 1.46 | 6.96 | 0.84 | 0.14 | 10.57 | 12.66 | 520.09 | 137.82 | 1159.25 | 65.33 | 938.04 | 249.81 | 95.67 | 61.61 | 552.73 | 24.58 | 122.41 | 11.33 | 366.24 | < 1 | 14.05 | 38.00 | 54.00 | 5.00 | |
| RSS38 | 2.06 | 14.41 | 6.71 | 52.67 | 0.10 | 1.09 | 4.41 | 0.95 | 0.11 | 11.57 | 8.90 | 293.45 | 179.76 | 2962.32 | 75.70 | 652.46 | 151.28 | 112.79 | 43.73 | 201.17 | 18.21 | 110.85 | 1.60 | 211.59 | 20.00 | 13.04 | 40.00 | 83.00 | 3.00 | |
| RSS40 | 1.25 | 16.06 | 6.90 | 50.25 | 0.10 | 1.12 | 4.21 | 0.83 | 0.15 | 13.14 | 9.70 | 254.15 | 172.77 | 2183.32 | 53.93 | 794.74 | 210.00 | 108.76 | 44.72 | 151.38 | 26.40 | 99.28 | 2.27 | 201.39 | 2.00 | 15.05 | 34.00 | 65.00 | 3.00 | |
| RSS41 | 0.70 | 21.54 | 5.83 | 43.33 | 0.07 | 0.53 | 8.26 | 0.68 | 0.10 | 12.25 | 10.51 | 659.03 | 168.13 | 2665.56 | 66.39 | 1205.28 | 282.41 | 98.63 | 25.69 | 171.88 | 18.47 | 76.35 | 2.56 | 58.23 | 5.00 | 10.01 | 29.00 | 108.00 | 2.00 | |
| RSS42 | 1.99 | 10.98 | 9.50 | 53.43 | 0.13 | 1.57 | 4.58 | 0.81 | 0.14 | 10.02 | 9.24 | 335.37 | 170.77 | 928.76 | 43.56 | 531.52 | 157.25 | 103.73 | 63.60 | 222.09 | 29.14 | 121.45 | 4.00 | 277.87 | < 1 | 17.06 | 39.00 | 65.00 | 6.00 | |
| RSS43 | 1.48 | 5.27 | 9.90 | 50.91 | 0.15 | 1.97 | 6.92 | 0.73 | 0.65 | 9.82 | 12.55 | 282.97 | 166.78 | 420.13 | 49.78 | 351.64 | 192.09 | 117.82 | 86.46 | 230.05 | 38.24 | 130.12 | 5.73 | 456.31 | < 1 | 29.10 | 37.00 | 53.00 | 4.00 | |
| RSS44 | 1.46 | 12.16 | 8.21 | 50.84 | 0.12 | 2.02 | 5.28 | 0.99 | 0.27 | 11.24 | 10.60 | 227.95 | 152.80 | 732.31 | 64.30 | 630.10 | 183.13 | 107.75 | 77.51 | 244.99 | 24.58 | 113.74 | 4.13 | 292.31 | 8.00 | 15.05 | 35.00 | 71.00 | 5.00 | |
| RSS46 | 0.91 | 15.76 | 5.98 | 49.66 | 0.09 | 0.97 | 1.95 | 0.66 | 0.16 | 16.69 | 10.69 | 339.30 | 140.81 | 7725.76 | 132.74 | 2620.00 | 573.27 | 141.99 | 38.76 | 208.14 | 20.03 | 85.79 | 4.13 | 265.12 | 7.00 | 11.04 | 41.00 | 67.00 | 4.00 | |

Table 1 (continued)

| CODE | Na ₂ O | MgO | Al ₂ O ₃ | SiO ₂ | P ₂ O ₅ | K ₂ O | CaO | TiO ₂ | MnO | Fe ₂ O ₃ | LOI | S | V | Cr | Co | Ni | Cu | Zn | Rb | Sr | Y | Zr | Nb | Ba | Hf | Pb | La | Ce | Th |
|-------|-------------------|-------|--------------------------------|------------------|-------------------------------|------------------|------|------------------|------|--------------------------------|-------|--------|--------|----------|--------|---------|--------|--------|-------|--------|-------|--------|------|--------|-------|-------|-------|-------|------|
| RSS47 | 0.20 | 28.93 | 0.53 | 37.33 | 0.01 | 0.30 | 0.66 | 0.17 | 0.11 | 21.73 | 12.50 | 285.59 | 50.93 | 22927.34 | 112.00 | 2453.33 | 403.08 | 166.16 | 20.87 | 94.61 | 0.00 | 40.48 | 6.27 | 103.67 | 47.00 | 5.02 | 19.00 | 93.00 | 1.00 |
| RSS49 | 1.89 | 12.76 | 7.95 | 51.52 | 0.12 | 1.08 | 3.30 | 0.84 | 0.14 | 12.59 | 8.90 | 323.58 | 200.73 | 1091.18 | 60.15 | 555.91 | 163.22 | 103.73 | 43.73 | 143.41 | 30.05 | 94.46 | 3.73 | 142.76 | <1 | 15.05 | 32.00 | 87.00 | 4.00 |
| RSS50 | 2.20 | 14.22 | 7.13 | 54.53 | 0.08 | 1.00 | 2.89 | 0.79 | 0.11 | 11.93 | 8.30 | 254.15 | 180.76 | 1410.16 | 70.52 | 632.13 | 151.28 | 116.82 | 45.71 | 119.51 | 19.12 | 95.42 | 0.67 | 131.71 | 17.00 | 15.05 | 32.00 | 90.00 | 3.00 |
| RSS51 | 2.39 | 11.07 | 9.54 | 51.97 | 0.16 | 1.58 | 6.32 | 0.88 | 0.13 | 10.18 | 7.99 | 247.60 | 201.73 | 700.22 | 40.44 | 384.16 | 135.36 | 95.67 | 67.58 | 243.00 | 28.22 | 127.23 | 3.33 | 316.10 | <1 | 14.05 | 40.00 | 54.00 | 5.00 |
| RSS52 | 2.37 | 8.00 | 10.74 | 50.19 | 0.22 | 2.01 | 5.38 | 0.94 | 0.16 | 12.51 | 5.86 | 169.00 | 246.67 | 439.58 | 48.74 | 243.91 | 127.39 | 88.62 | 69.56 | 421.27 | 42.79 | 135.91 | 9.33 | 480.10 | <1 | 12.04 | 57.00 | 75.00 | 6.00 |
| RSS53 | 2.52 | 13.40 | 7.14 | 54.66 | 0.11 | 1.19 | 3.58 | 0.81 | 0.13 | 9.55 | 8.60 | 301.31 | 166.78 | 1109.65 | 85.04 | 614.86 | 160.24 | 111.78 | 52.67 | 209.14 | 18.21 | 101.21 | 2.53 | 188.64 | 32.00 | 15.05 | 39.00 | 95.00 | 5.00 |

classical statistical methods are dependent on the supposition of normality of the data, and no normal distribution of the data could lead to biased and wrong results (Reimann and Filzmoser 2000). In the normal populations, the kurtosis is around three, skewness zero, and the amount of mean, mode, and median are the same. To find out the normal distribution of the data, histograms, scatter plot, boxplot, and Q–Q plots of elements are generated (Figs. 4, 5, 6). According to the plots, V has a normal distribution, but Ba, Co, Cr, Cu, Ni, Pb, and Zn do not indicate normal distribution, but rather the element plots are comprised of multiple populations indicating that the researched area probably was exposed to variable geological events (Zuo 2011; Daya and Afzal 2015).

To normalize the data, ln-transformation was applied (Figs. S1, s2, and s3), and the processed data (Table 2) show now a normal or near-normal distribution ready for further processing by classical methods.

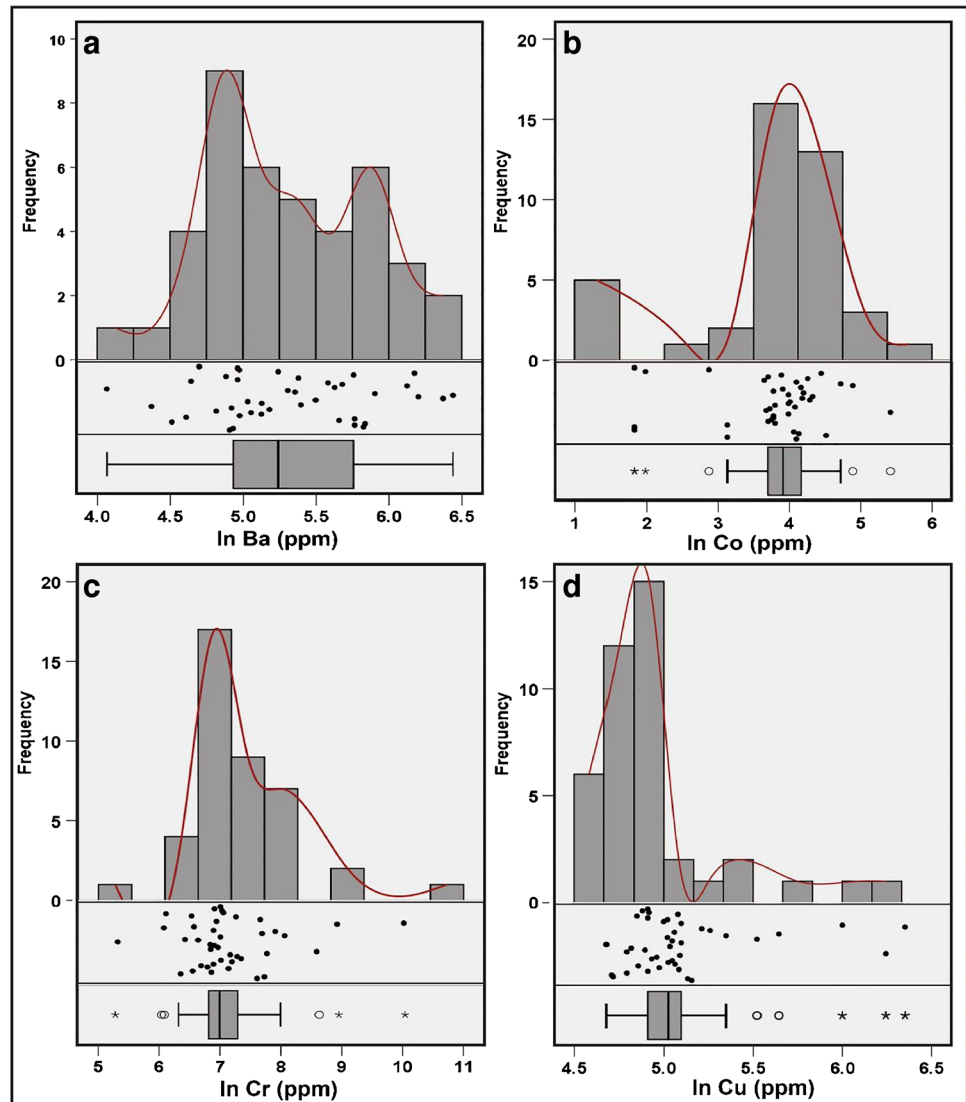
Correlation

To identify the inter-relations between the studied elements in univariate analysis, the Spearman correlation coefficient has been used since it is robust against data outliers, and the results from original data and linear transformation will be similar. Table 3 shows the correlation coefficient for different elements. The results show a strong positive correlation between Cr and Ni and less evident with Cu; this correlation might be due to presence of ultramafic rocks in the area. Cr also has a good correlation with Mg, probably because of co-occurrence in the same lithology or mineral phases (e.g. Cr-Mg-spinels). A good positive correlation among Rb, Sr, Ba, Al₂O₃, and K₂O indicates their clustering in silicates like feldspars and/or clay minerals such as fuchsite occurring in the broader area (Pirouei et al. 2020).

Geochemical mapping of the elements with different methods

Various statistical methods have been employed to separate anomalies from the background, and consequently to map the distribution of the elements (e.g. Hawkes and Webb 1962; Cheng et al. 1994). In this study, classical statistical methods (M + 2MAD and TIF) and the fractal method (C-A) were used. The Digital Elevation Model (DEM) was used to draw the basins and drainage system of the studied area. The geochemical maps were designed according to background and anomalies classes and the respective basins by using ArcGIS 10.6 (Figs. s4-s7, 7 and 8).

Fig. 4 Histograms and EDA graphics (density trace, jittered one-dimensional scatterplots, and boxplots) of (a) Ba, (b) Co, (c) Cr, and (d) Cu showing no normal distribution



M + 2MAD method

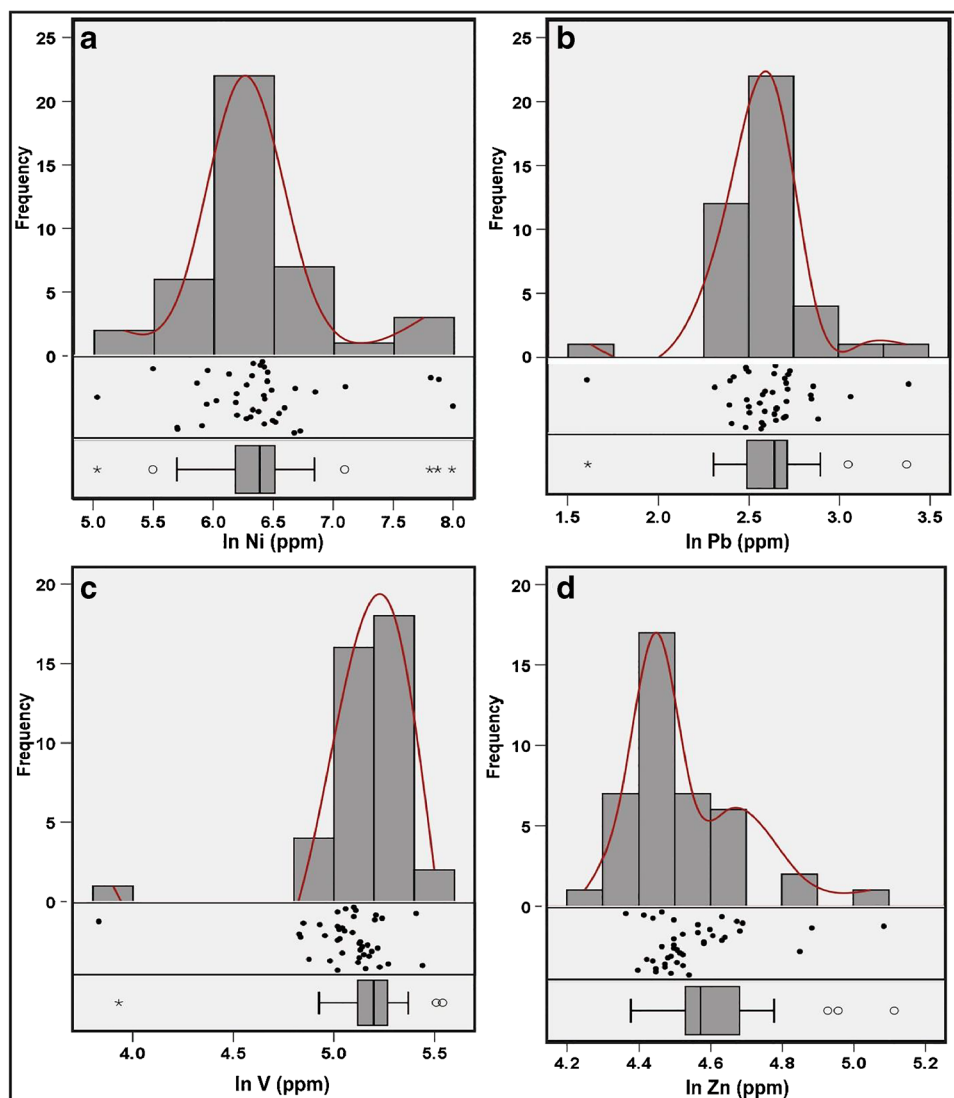
This method depends on the median (M) and median absolute deviation (MAD) calculations on the normalized data (Reimann et al. 2005). According to this MAD, which is comparable to the method of $X + 2S$ (Hawkes and Webb 1962; Matschullat et al. 2000), the amount of $M + 2MAD$ is considered the threshold for anomalies. In the Rayat area, the background and the anomalies thresholds were calculated as follows (Table s1): (1) the values $< M$ are considered low background; (2) the values between M and $M + MAD$ are considered background; (3) the values between $M + MAD$ and $M + 2MAD$ are considered high background; (4) the values between $2M + MAD$ and $M + 3MAD$ are considered anomalies; (5) the values $> M + 3MAD$ are considered strong anomalies. According to the calculation, five classes are determined for each element (presented in Table s2).

The geochemical map of elements distribution (Figs. s4 and s5) shows strong anomalies for Ba, Co, Cr, Cu, Ni, and Zn in the southern part of the studied area. Lead shows strong anomalies in north and south parts, and V shows strong anomalies in the NW and W part of the area. Also, Ba, Co, Cr, Cu, Ni, and Pb show weaker anomalies in some parts of the area (Figs. s4 and s5).

Tukey's inner fences method

According to the statistical calculation on the geochemical data by Tukey's boxplot (Table s3), five classes are proposed for each element (Table s4). The threshold between high background and anomalies of Ba, Co, Cr, Cu, Ni, Pb, V, and Zn is 1089.84, 128.88, 2989.34, 216.14, 1104.83, 21.03, 234.19, and 135.15 respectively. Based on geochemical maps, Ba does not show any anomaly in the area and the values of Ba reach the

Fig. 5 Histograms and EDA graphics (density trace, jittered one-dimensional scatterplots, and boxplots) of (a) Ni, (b) Pb, (c) V, and (d) Zn. Only vanadium (V) histogram appears to be symmetric and with normal distribution



high background (Fig. s6a). Cobalt indicates a strong and a weak anomaly in the SE and SW part of the Rayat, respectively (Fig. s6b). Chromium displays a strong anomaly in the SW part, whereas it demonstrates a weak anomaly in the SE of the area (Fig. s6c). Cu and Ni depict two strong anomalies in the SW and SE of the area (Figs. s6d and s7a). The strong anomaly of the Pb can be observed in the SW of the area (Fig. s7b). Vanadium and Zn show weak anomalies in the West part and South part of the region, respectively (Fig. s7c and d).

Fractal method

Based on the distribution maps of Ba, Co, Cr, Cu, Ni, Pb, V, and Zn produced with ArcGIS 10.6 (Figs. 7, 8), the C-A plots were obtained. The zinc plot suggests seven enrichment stages (fig. s8a). The values of 93.33 and 104.71 are the lowest enrichment stage; the values of

120.22 and 143.88 are moderate, whereas the values of 158.49 and 164.44 are the highest enrichment steps of this element. The plot of Ni indicates six enrichment stages (Fig. s8b) with threshold values (Table s5). Low and moderate Ni enrichment stages were below 110.41 ppm and between 121.62 and 213.8 ppm, respectively. The high enrichment stage of Ni is above 240.1 ppm. According to the Cu plot (Fig. s8c), this element shows four enrichment stages with threshold values (Table s5). The population among 165–181 were moderate and those above 181 ppm represent the moderate enrichment stages of V (Fig. s8d). Also, the concentration of more than 245 is high enrichment steps of V (Table s5).

According to Pb plot, this element shows six enrichment stages (Fig. s9a). The lowest threshold of Pb are between 14.52 and 15.14, and moderate threshold values are between 17.78 and 26.3, and the highest threshold value of lead is 28.18. The chromium plot demonstrates

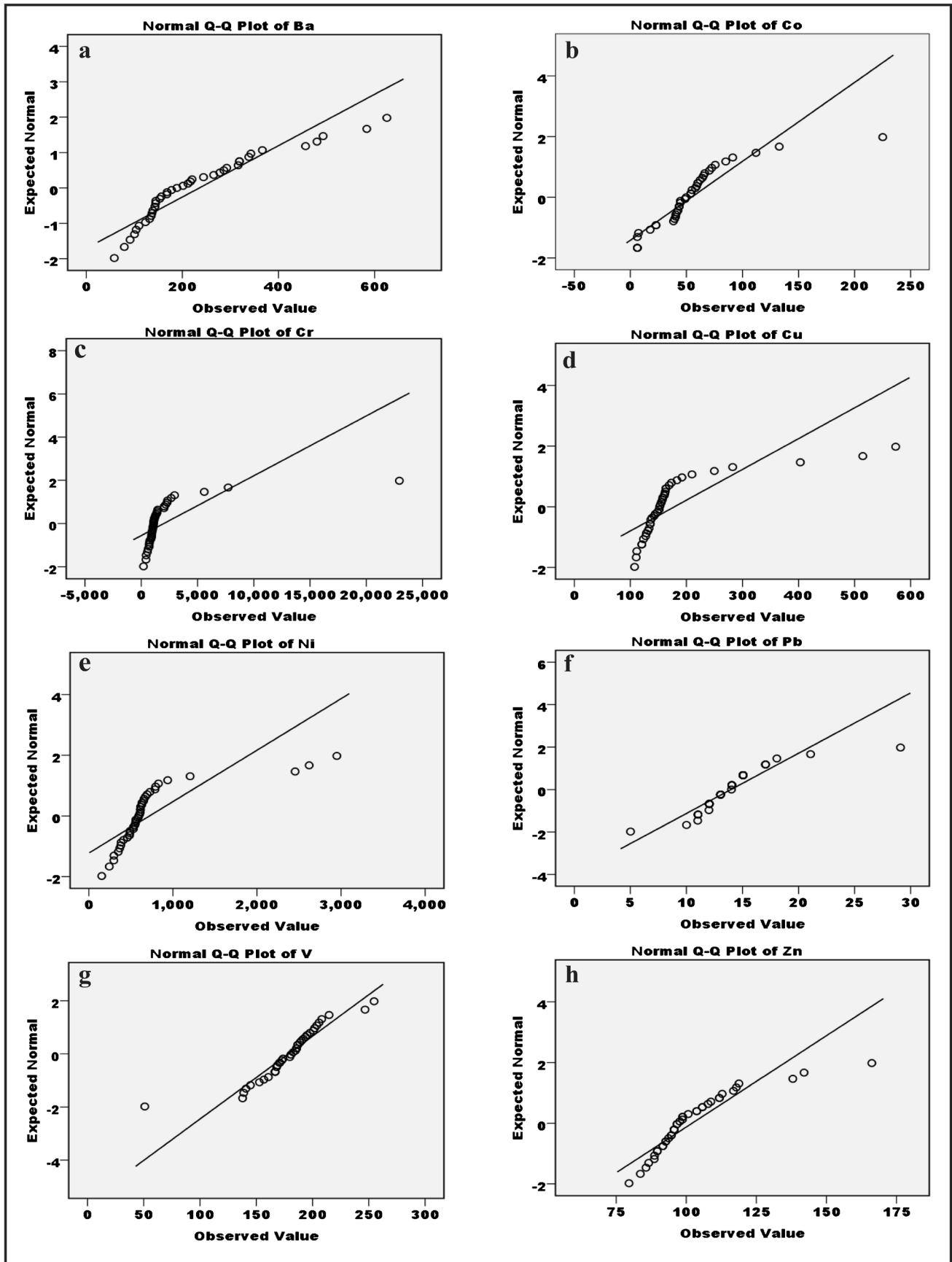


Fig. 6 Normal Q-Q plot of (a) Ba, (b) Co, (c) Cr, (d) Cu, (e) Ni, (f) Pb, (g) V, and (h) Zn. All the elements show deviation from the normal distribution (straight line), except for vanadium which shows a normal distribution

six enrichment stages (Fig. s9b). The lowest threshold value is 246 and 2138; the moderate is 3162.3 and 10,471.7, and the highest threshold value is 19059.7 (Table s5). According to the plot, there are five enrichment stages (Fig. s9c) for Ba within the threshold amounts of 208.93, 309.03, 549.54, and 616.6 ppm (Table s5). Cobalt plot denotes six enrichment stages (Fig. s9d and Table s5), the lowest enrichment steps are between 28.58 and 29.85. The moderate enrichment steps are between 87.1 and 97.72, while the highest is 194.99.

According to C-A log–log plots of Cr, Ni, Cu, Pb, and Co, six geochemical populations are regarded as low, moderate, and high background, as well as weak, high, and extreme anomaly. Barium and vanadium plots show five populations as low, moderate, and high background, weak anomaly, and high anomaly. Moreover, Zn shows seven populations as very low, low, moderate, and high background as well as weak, high, and extreme anomalies. According to the threshold obtained by C-A log–log plots, ArcGIS produced distribution maps of each element to show probable anomalies in the area (Figs. 7 and 8).

Based on the constructed geochemical maps by (C-A) fractal method, Ba, Cr, Cu, Pb, and Zn show a strong anomaly in the SW of the area (Figs. 7a, c, d and 8b, d). Cobalt and Ni show strong anomalies in the SE and weak anomalies in the SW of the area (Fig. 7b and 8a). Vanadium indicates a strong anomaly in the Western part of the area (Fig. 8c).

Discussion

Statistical evaluation—factor analyses and geogenic influence in the geochemical features of stream sediments

Factor analysis (Davis 1986) was used to obtain a grouping of elements within the samples based on their geochemical associations by utilizing the software of IBM SPSS®. The results showed a 5-factor model which covers 82% of the overall variance of the eigenvalues, that all of them showing a bipolar mode (Table s6). By correlating the factor loadings, seven groups and associations were gained as follows (Fig. 9a): G1: K, Sr, Nb, Ba; G2: S, Co, Ni, Cu, and Zn; G3: P, Fe, Cr, and Zn; G4: Cr, Ni, and LOI; G5: V, Ti, and Ca; G6: Al, P, Zr, and La; and G7: Na, Si, Ti, and V.

A strong positive correlation between Cr and Ni (Fig. 9b) might be related to their concentration in the mafic and ultramafic rocks. The supergene alteration also can accumulate Cr and Ni together. These two elements show high concentrations in the samples of the Rayat area, especially in two locations in the southern part of the area influenced probably by the volcano-sedimentary rocks of the Walsh Group. The Walsh Group contains chromite mineralization (Ismail et al. 2009), and it is also affected by hydrothermal multiphase activity (Pirouei et al. 2020). Moreover, the occurrence of weathered serpentinized peridotite, as alteration products of peridotite, may have provided lateritic mineralizations (e.g. garnierite), which can increase the amount of Ni in the stream sediments. S, Co, Ni, Cu, and Zn are linked together in G2 (Fig. 9); they might reflect the presence of

Table 2 Statistical parameters of the Rayat stream sediment samples

| Parameters | V (ppm) | Ln_Cr (ppm) | Ln_Co (ppm) | Ln_Ni (ppm) | Ln_Cu (ppm) | Ln_Zn (ppm) | Ln_Ba (ppm) | Ln_Pb (ppm) |
|------------------------|---------|-------------------|-------------------|-------------|-------------|-------------|-------------|-------------|
| Mean | 178.61 | 7.13 | 3.74 | 6.39 | 5.10 | 4.61 | 5.31 | 2.61 |
| Std. Error of mean | 5.01 | 0.13 | 0.13 | 0.09 | 0.06 | 0.02 | 0.09 | 0.04 |
| Median | 180.76 | 7.00 | 3.91 | 6.39 | 5.02 | 4.57 | 5.24 | 2.64 |
| Mode | 166.78 | 5.28 ^a | 1.83 ^a | 6.42 | 4.91 | 4.56 | 4.96 | 2.71 |
| Std. Deviation | 32.05 | 0.80 | 0.83 | 0.56 | 0.37 | 0.15 | 0.56 | 0.25 |
| Variance | 1027.21 | 0.65 | 0.70 | 0.32 | 0.14 | 0.02 | 0.31 | 0.06 |
| Skewness | -1.15 | 1.28 | -1.14 | 0.90 | 2.11 | 1.42 | 0.12 | -0.79 |
| Std. Error of skewness | 0.37 | 0.37 | 0.37 | 0.37 | 0.37 | 0.37 | 0.37 | 0.37 |
| Kurtosis | 5.97 | 4.02 | 1.26 | 2.60 | 4.61 | 2.76 | -0.48 | 7.31 |
| Std. Error of kurtosis | 0.72 | 0.72 | 0.72 | 0.72 | 0.72 | 0.72 | 0.72 | 0.72 |
| Range | 203.73 | 4.76 | 3.59 | 2.96 | 1.67 | 0.74 | 2.37 | 1.76 |
| Minimum | 50.93 | 5.28 | 1.83 | 5.03 | 4.68 | 4.38 | 4.06 | 1.61 |
| Maximum | 254.66 | 10.04 | 5.42 | 7.99 | 6.35 | 5.11 | 6.44 | 3.37 |
| Sum | 7322.89 | 292.48 | 153.15 | 262.18 | 209.06 | 189.20 | 217.58 | 106.92 |

Table 3 Spearman's correlation coefficient of the elements in the of the Rayat area stream sediment samples

| | Na ₂ O | MgO | Al ₂ O ₃ | SiO ₂ | P ₂ O ₅ | K ₂ O | CaO | TiO ₂ | MnO | Fe ₂ O ₃ | V | Cr | Co | Ni | Cu | Zn | Rb | Sr | Ba | Pb | |
|--------------------------------|-------------------|-------|--------------------------------|------------------|-------------------------------|------------------|-------|------------------|-------|--------------------------------|-------|-------|-------|-------|-------|-------|------|-------|------|------|--|
| Na ₂ O | 1.00 | | | | | | | | | | | | | | | | | | | | |
| MgO | -0.40 | 1.00 | | | | | | | | | | | | | | | | | | | |
| Al ₂ O ₃ | 0.45 | -0.93 | 1.00 | | | | | | | | | | | | | | | | | | |
| SiO ₂ | 0.50 | -0.22 | 0.17 | 1.00 | | | | | | | | | | | | | | | | | |
| P ₂ O ₅ | 0.41 | -0.86 | 0.90 | 0.08 | 1.00 | | | | | | | | | | | | | | | | |
| K ₂ O | 0.52 | -0.79 | 0.82 | 0.40 | 0.84 | 1.00 | | | | | | | | | | | | | | | |
| CaO | -0.20 | -0.29 | 0.17 | -0.43 | 0.19 | -0.10 | 1.00 | | | | | | | | | | | | | | |
| TiO ₂ | 0.52 | -0.28 | 0.41 | 0.15 | 0.55 | 0.50 | 0.01 | 1.00 | | | | | | | | | | | | | |
| MnO | 0.22 | -0.52 | 0.60 | 0.17 | 0.68 | 0.76 | -0.31 | 0.33 | 1.00 | | | | | | | | | | | | |
| Fe ₂ O ₃ | -0.11 | 0.51 | -0.33 | -0.10 | -0.22 | -0.14 | -0.56 | 0.22 | 0.15 | 1.00 | | | | | | | | | | | |
| V | 0.28 | -0.15 | 0.19 | 0.31 | 0.18 | 0.06 | 0.21 | 0.51 | -0.19 | 0.04 | 1.00 | | | | | | | | | | |
| Cr | -0.42 | 0.85 | -0.82 | -0.33 | -0.72 | -0.82 | -0.04 | -0.29 | -0.50 | 0.37 | -0.04 | 1.00 | | | | | | | | | |
| Co | 0.05 | 0.18 | -0.11 | -0.10 | 0.01 | -0.01 | -0.31 | 0.09 | 0.18 | 0.23 | -0.19 | 0.18 | 1.00 | | | | | | | | |
| Ni | -0.62 | 0.73 | -0.75 | -0.44 | -0.66 | -0.69 | -0.09 | -0.49 | -0.29 | 0.21 | -0.53 | 0.73 | 0.21 | 1.00 | | | | | | | |
| Cu | -0.52 | 0.48 | -0.44 | -0.48 | -0.33 | -0.35 | -0.15 | -0.42 | 0.10 | 0.29 | -0.55 | 0.51 | 0.40 | 0.77 | 1.00 | | | | | | |
| Zn | 0.02 | 0.30 | -0.16 | -0.19 | -0.14 | -0.04 | -0.46 | -0.06 | 0.31 | 0.35 | -0.46 | 0.28 | 0.50 | 0.36 | 0.60 | 1.00 | | | | | |
| Rb | 0.28 | -0.79 | 0.74 | 0.26 | 0.69 | 0.79 | 0.07 | 0.16 | 0.54 | -0.43 | -0.16 | -0.90 | -0.21 | -0.52 | -0.37 | -0.20 | 1.00 | | | | |
| Sr | 0.36 | -0.77 | 0.71 | -0.03 | 0.76 | 0.65 | 0.42 | 0.40 | 0.40 | -0.36 | 0.09 | -0.61 | 0.01 | -0.53 | -0.34 | -0.28 | 0.55 | 1.00 | | | |
| Ba | 0.30 | -0.77 | 0.74 | 0.09 | 0.83 | 0.80 | 0.04 | 0.34 | 0.74 | -0.21 | -0.14 | -0.72 | 0.12 | -0.47 | -0.19 | 0.03 | 0.77 | 0.76 | 1.00 | | |
| Pb | 0.23 | -0.29 | 0.31 | 0.40 | 0.25 | 0.46 | -0.33 | -0.02 | 0.50 | -0.18 | -0.34 | -0.49 | -0.21 | -0.15 | -0.03 | 0.18 | 0.58 | -0.08 | 0.32 | 1.00 | |

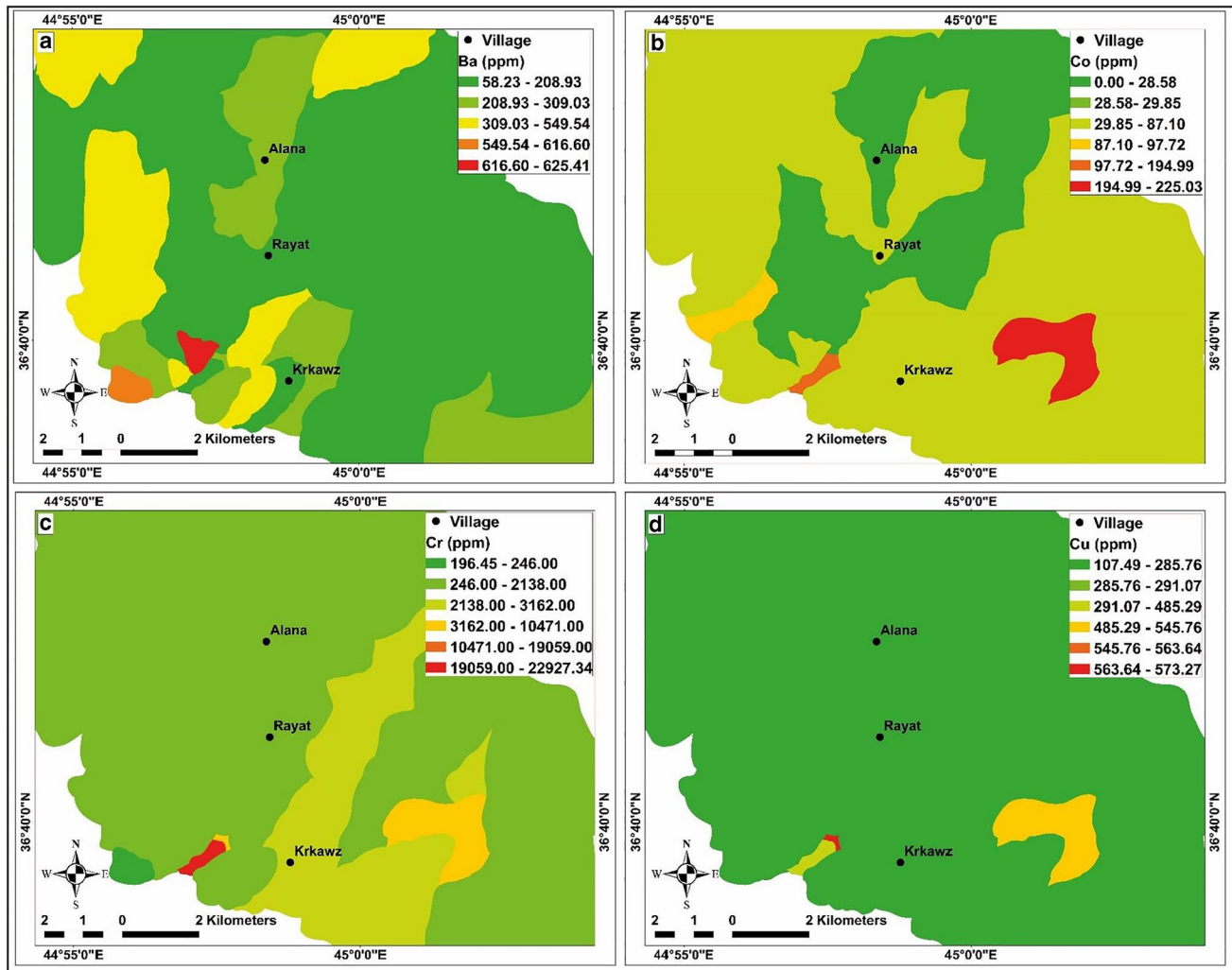


Fig. 7 Geochemical distribution maps of (a) Ba, (b) Co, (c) Cr, and (d) Cu obtained by the concentration-area fractal method

mineralizations in the form of sulphide minerals (possibly in the form of hydrothermal or VMS deposits) within the mafic and ultramafic rocks of the Walsh group. Their geochemical distribution maps show similar spatial distribution (Figs. s6 and s7). Grouping of K, Sr, Nb, Ba together may indicate their affiliation in feldspar and/or fuchsite, which has been reported in the area recently (Pirouei et al. 2020).

Iron is grouped with Cr, P, and Zn in G3. This association corresponds probably to the presence of newly discovered iron ore in the area in the form of gossanite over layers rich in sulphide minerals (Pirouei et al. 2021). The other sources of Fe can be the basalt, ferruginous breccia, and conglomerate that are abundant in the study area. V, Ti, and Ca are grouped together in G5, probably reflecting the presence of spilite and basalt in the area that contains titanomagnetite, pyroxene, and feldspars and to lesser amount might be due to presence of serpentine.

From the presented geochemical data, it can be concluded that there is indication of robust geogenic control in the dispersion of the studied elements in the samples of the Rayat area. The strong correlation between Cu and Zn (Fig. 9c) could be an indicator of sulphide mineralization in the area that occurred in the lower part of gossanite (Pirouei et al. 2021). A moderate to strong correlation between Fe and Cr can represent either their association in the ultramafic or the occurrence of chromitite in the area (Fig. 9d).

Validity of the determined background concentrations

The threshold values obtained by the three methods employed here show some differences. The background amount achieved by the methods shows a diminishing concentration order $C-A > TIF > MAD$ (Tables s1, s3,

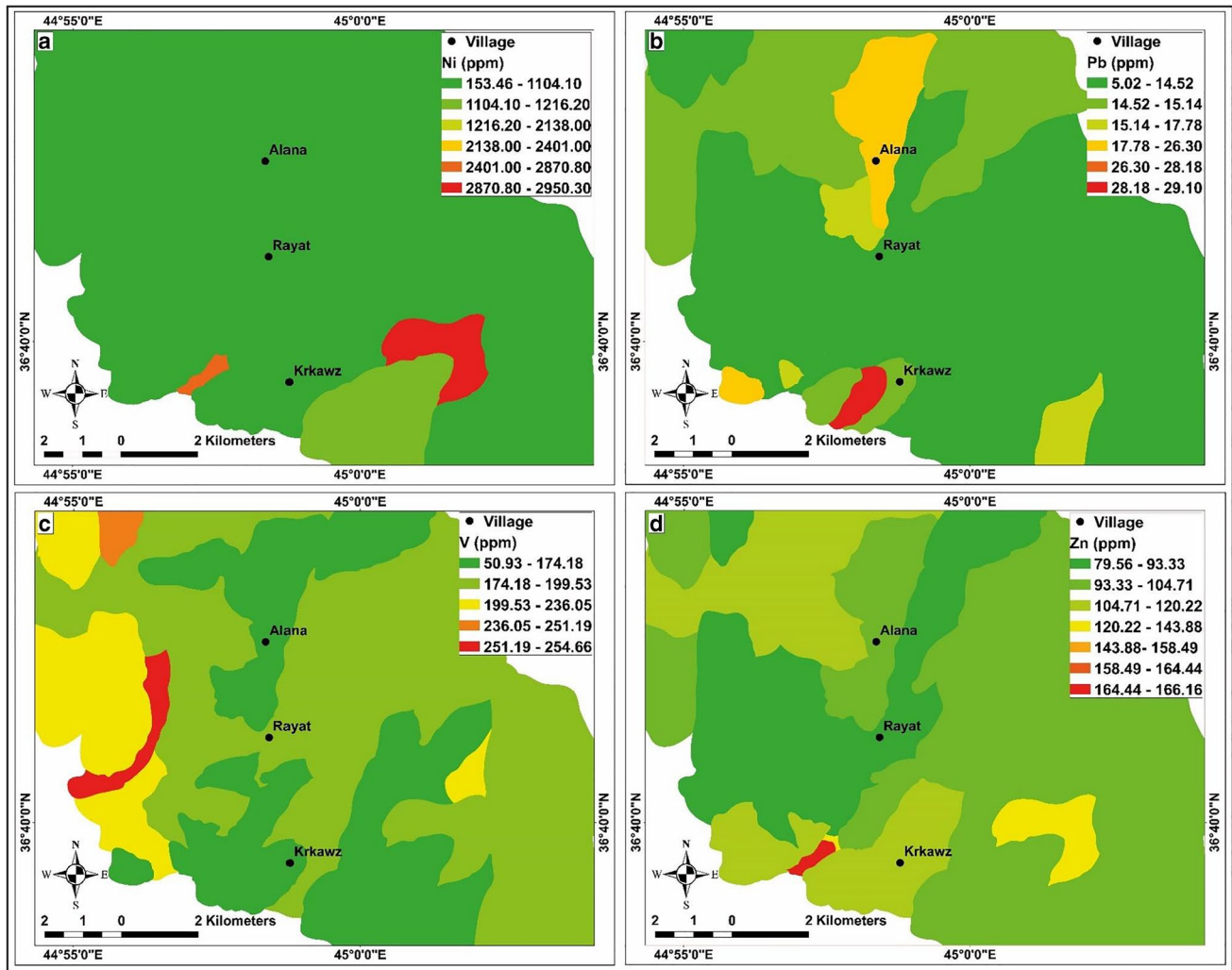


Fig. 8 Geochemical distribution maps of (a) Ni, (b) Pb, (c) V, and (d) Zn obtained by the concentration-area fractal method

and s5). In general, the evaluation of the geochemical maps constructed by the three procedures gave almost the same results for the different elements. The main differences are described below:

Ba: the fractal method shows a strong anomaly, whereas the MAD method shows weak anomalies, and the TIF method does not show any anomalies.

Cr: MAD shows two sites of strong anomalies in the area, whereas the two other methods show one site of strong anomalies.

Cu and Ni: TIF and MAD methods show two strong anomalies in two places, whereas the fractal method shows only one.

Pb: fractal method reveals one region of the anomaly, but TIF shows one place with strong and another with

weak anomalies, and the MAD method shows two strong anomalies with one weak anomaly.

V: MAD and fractal show strong anomalies whereas TIF does not show strong anomalies.

Zn: according to the MAD method, two strong anomalies are indicated in the area, whereas fractal provides only one strong anomaly, and TIF shows two weak anomalies in the area.

The assessment of the three methods shows that the above differences do not affect the outcome significantly. The MAD procedure has been broadly debated in the literature (Reimann et al. 2005; Reimann and de Caritat 2017). Background amounts resulted from the MAD method are widely expressed as representing the environmental background (Reimann et al. 2005). The TIF

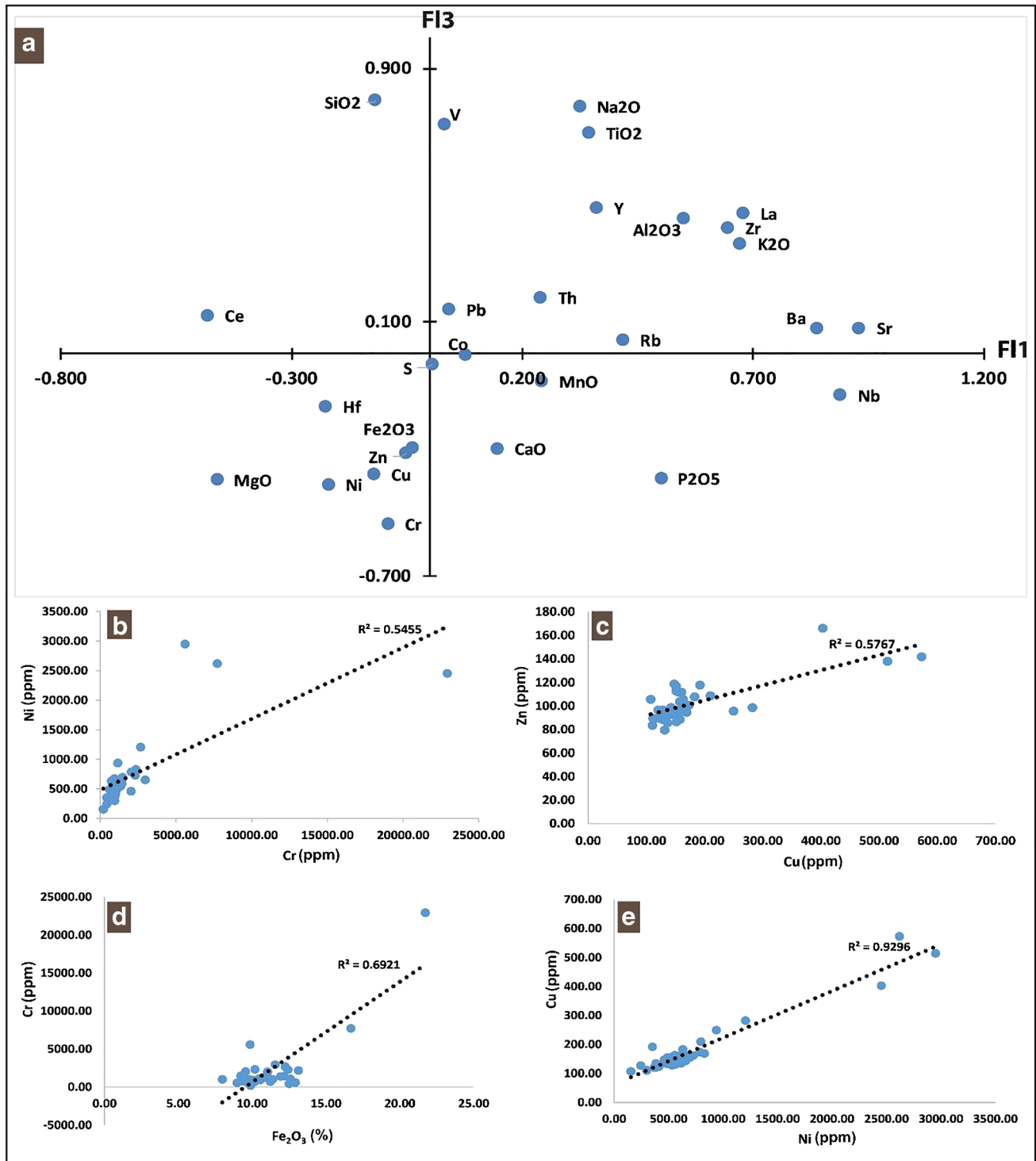
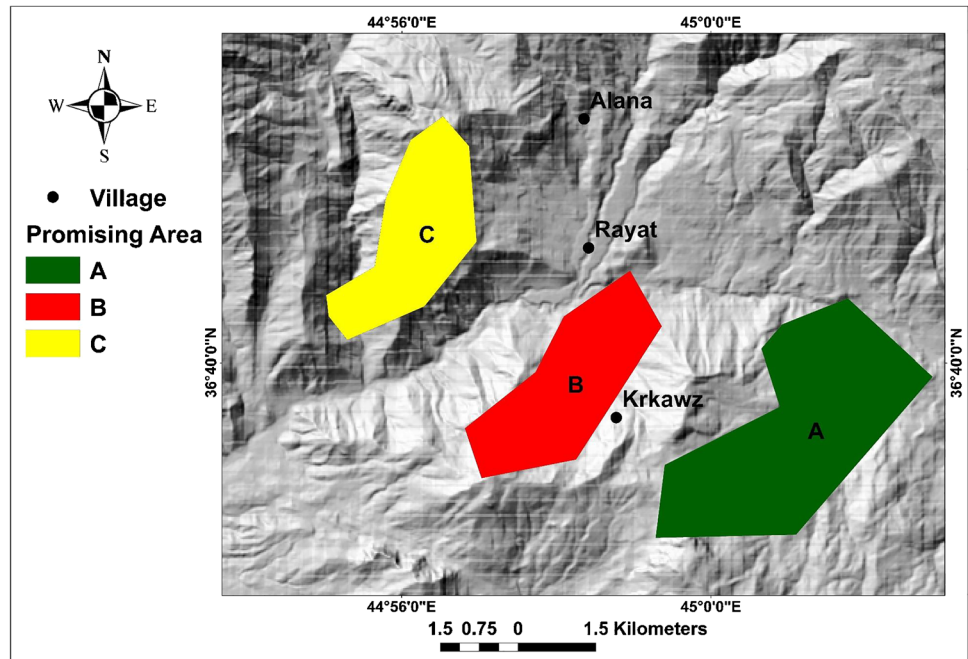


Fig. 9 a R-type scatter plot of the 1st (FL1) vs. the 3rd (FL3) factor loadings; (b) regression analysis scatter plot of Cr vs. Ni; (c) regression analysis scatter plot of Cu vs. Zn; (d) regression analysis scatter plot of Fe₂O₃ vs. Cr; and (e) regression analysis scatter plot of Ni vs. Cu

method is suitable in projects, in which the numbers of outliers are less than 15% (Reimann et al. 2018), In this research, the number of outliers is less than 15%; thus, the

usage of the TIF method is beneficial. Generally, utilizing the TIF method for initial class selection to demonstrate spatial data structure in a map has been confirmed to be

Fig. 10 Promising areas (A, B, and C) for the next exploration projects



a reliable tool for recognizing the crucial geochemical processes behind a data distribution. Concentration-area (C-A) fractal method, as it considers the spatial distribution of the elements besides their frequency, is widely used by researchers in recent years (Daya and Afzal 2015; Afzal et al. 2017; Ghezlbash et al. 2019). In this research, the fractal method shows different thresholds and consequently different populations, somehow better than of classical methods for some elements of interest. For example, the classical methods that were used in this research did not show any strong anomalies for the barium, whereas the C-A method shows a strong anomaly of Ba in SE of the Rayat area.

Implications for mineral exploration and defining promising mineralization areas

The geochemical maps obtained in three locations in the broader Rayat area demonstrate the presence of high anomalies that can be an essential guide for the geochemical exploration of new ore deposits and economic significance for the development of the area. The occurrence of mafic and ultramafic rocks in the area (Mohammad 2009; Ismail et al. 2009) might be associated with primary magmatic mineralizations. Additionally, listvenitization in the area (Pirouei et al. 2020) is an indicator of hydrothermal activity that could lead to the occurrence of hydrothermal-related ore deposits in the Rayat area.

Anomalous concentrations of Cr, Ni, Cu, and Zn have been identified in the south of the Rayat area, where spatially are accompanied by the mafic and ultramafic rocks of the Walsh group. These ultramafic rocks, combined with the intense weathering, can be the source of the identified geochemical anomalies in the stream sediments, demonstrating possible evidence of chromium and Nickel ore deposits (Golightly 1981). Also, the co-occurrence of Ba, Pb, Zn, Cu, and Co in the same area may indicate hydrothermal mineralization of sulphide ore deposits in the area (Pirouei et al. 2021). Vanadium also shows a strong anomaly in the area that also can be related to the ultramafic rocks and magnetite-hematite mineralizations of the area. Finally, by superimposing the geochemical maps, three promising areas (A, B, and C) for future investigation can be proposed, as shown in Fig. 10. Places A and B are promising areas for the exploration of Cr, Ni, Cu, Pb, Zn, and Ba. Place C is a promising area for the exploration of vanadium.

Conclusions

The geochemical study of stream sediments in the Rayat area, Iraqi Kurdistan by using classical and fractal methods, proved a powerful tool to delineate potential mineralization areas, particularly towards the south-south-eastern of Rayat village. The main conclusions of this research are as follows:

1. The anomalies in the studied area can be correlated with the occurrence of Eocene–Oligocene intrusions, ophiolitic terrain, and volcanic rocks.
2. The main types of proved mineralizations include primary magmatic Cr-Fe-V, gossanite, and potential mineralizations that could be considered are supergene Cr-Ni-Fe, laterite, and VMS-related hydrothermal Cu-Pb-Zn sulphides.
3. The obtained data represent an initial knowledge-based effort for more versatile management of the natural resources of the Rayat area in the Kurdistan Region, Iraq.
4. According to both classical and C-A fractal methods, there are three main promising areas of anomalies for the next investigations. They are located in the NW, S, and SE of the Rayat village.
5. Based on the C-A log–log plots, it can be concluded that all studied elements show different levels of enrichment, i.e. mineralization and later dispersions.
6. The results of both classic and fractal methods demonstrate that classic methods can still be used for geochemical exploration purposes.

Supplementary Information The online version contains supplementary material available at <https://doi.org/10.1007/s12517-022-09778-w>.

Acknowledgements Dr. Vaya Xanthopoulou, Laboratory of Electron Microscopy and Microanalysis, Faculty of Natural Sciences, University of Patras, is acknowledged for the XRF analysis. The authors would also like to thank the anonymous reviewers for their valuable comments and suggestions.

Declarations

Competing interests There are no known competing financial interests or personal relationships that could have appeared to influence the work reported in this paper.

References

- Afzal P, Yasrebi A, Saein L, Panahi S (2017) Prospecting of Ni mineralization based on geochemical exploration in Iran. *J Geochemical Explor* 181:294–304
- Aswad KJA, Aziz NRH, Koyi HA (2011) Cr-spinel compositions in serpentinites and their implications for the petrotectonic history of the Zagros Suture Zone, Kurdistan Region, Iraq. *Geol Mag* 148:802–818. <https://doi.org/10.1017/S0016756811000422>
- Bai J, Porwal A, Hart C et al (2010) Mapping geochemical singularity using multifractal analysis: application to anomaly definition on stream sediments data from Funin Sheet, Yunnan, China. *J Geochemical Explor* 104:1–11. <https://doi.org/10.1016/j.gexplo.2009.09.002>
- Bölviken B, Björklund A, Kontio M, et al (1986) Geochemical atlas of Northern Fennoscandia. *Geol Surv Finland, Norw Sweden*
- Bounessah M, Atkin BP (2003) An application of exploratory data analysis (EDA) as a robust non-parametric technique for geochemical mapping in a semi-arid climate. *Appl Geochemistry* 18:1185–1195. [https://doi.org/10.1016/S0883-2927\(02\)00247-0](https://doi.org/10.1016/S0883-2927(02)00247-0)
- Changjiang L, Ma T, Shi J (2003) Application of a fractal method relating concentrations and distances for separation of geochemical anomalies from background. *J Geochemical Explor* 77:167–175. [https://doi.org/10.1016/S0375-6742\(02\)00276-5](https://doi.org/10.1016/S0375-6742(02)00276-5)
- Chen X, Zheng Y, Xu R et al (2016) Application of classical statistics and multifractals to delineate Au mineralization-related geochemical anomalies from stream sediment data: a case study in Xinghai-Zeku, Qinghai, China. *China* 16:253–264. <https://doi.org/10.1144/geochem2016-424>
- Cheng Q (1999) Spatial and scaling modeling for geochemical anomaly separation. *J Geochemical Explor* 65:175–194. [https://doi.org/10.1016/S0375-6742\(99\)00028-X](https://doi.org/10.1016/S0375-6742(99)00028-X)
- Cheng Q, Agterberg FP, Ballantyne SB (1994) The separation of geochemical anomalies from background by fractal methods. *J Geochemical Explor* 51:109–130. [https://doi.org/10.1016/0375-6742\(94\)90013-2](https://doi.org/10.1016/0375-6742(94)90013-2)
- Cheng Q, Xu Y, Grunsky E (2000) Integrated spatial and spectrum method for geochemical anomaly separation. *Nonrenewable Resour* 9:43–52. <https://doi.org/10.1023/A:1010109829861>
- Davis JC (1986) *Statistics and data analysis in geology*. Wiley & Sons, New York
- Daya AA, Afzal P (2015) A comparative study of concentration-area (C-A) and spectrum-area (S-A) fractal models for separating geochemical anomalies in Shorabhazi region, NW Iran. *Arab J Geosci* 8:8263–8275. <https://doi.org/10.1007/s12517-014-1771-6>
- Ghezelbash R, Maghsoudi A (2018) Comparison of U -spatial statistics and C-A fractal models for delineating anomaly patterns of porphyry-type Cu geochemical signatures in the Varzaghan district, NW Iran. *Comptes Rendus Geosci* 350:180–191. <https://doi.org/10.1016/j.crte.2018.02.003>
- Ghezelbash R, Maghsoudi A, Daviran M, Yilmaz H (2019) Incorporation of principal component analysis, geostatistical interpolation approaches and frequency-space-based models for portraying the Cu-Au geochemical prospects in the Feizabad district, NW Iran. *Chem Erde* 79:323–336. <https://doi.org/10.1016/j.chemer.2019.05.005>
- Golightly J (1981) Nickeliferous laterite deposits. *Economic Geology*, 75th Anniv, pp 710–735
- Hawkes H, Webb J (1962) *Geochemistry in mineral exploration*, first edit. Harper and Row, New York
- Heiri O, Lotter A, Lemcke G (2001) Loss on ignition as a method for estimating organic and carbonate content in sediments: reproducibility and comparability of results. *J Paleolimnol* 25:101–110. <https://doi.org/10.1023/A:1008119611481>
- Hoaglin D, Mosteller F, Tukey J (2000) *Understanding robust and exploratory data analysis*, second. Wiley & Sons, New York
- Ismail SA, Arai S, Ahmed AH, Shimizu Y (2009) Chromitite and peridotite from Rayat, northeastern Iraq, as fragments of a Tethyan ophiolite. *Isl Arc* 18:175–183
- Kürzl H (1988) Exploratory data analysis: recent advances for the interpretation of geochemical data. *J Geochemical Explor* 30:309–322. [https://doi.org/10.1016/0375-6742\(88\)90066-0](https://doi.org/10.1016/0375-6742(88)90066-0)
- Mao Z, Peng S, Lai J et al (2004) Fractal study of geochemical prospecting data in south area of Fenghuanshan copper deposit, Tongling Anhui. *J Earth Sci Environ* 26:11–14
- Matschullat J, Ottenstein R, Reimann C (2000) Geochemical background - can we calculate it? *Environ Geol* 39:990–1000. <https://doi.org/10.1007/s002549900084>
- Mohammad YO (2009) Serpentinites and their tectonic signature along the Northwest Zagros Thrust Zone, Kurdistan Region, Iraq. *Arab J Geosci* 4:69–83. <https://doi.org/10.1007/s12517-009-0080-y>

- Mrvic VV, Kostić Kravljanac LM, Zdravković MS et al (2010) Background limit of Zn and Hg in soils of Eastern Serbia. *J Agric Sci* 55:157–163. <https://doi.org/10.2298/JAS1002157M>
- Parsa M, Maghsoudi A, Ghezelbash R (2016) Decomposition of anomaly patterns of multi-element geochemical signatures in Ahar area, NW Iran: a comparison of U-spatial statistics and fractal models. *Arab J Geosci* 9:260. <https://doi.org/10.1007/s12517-016-2435-5>
- Pirouei M, Kolo K, Kalaitzidis SP (2020) Hydrothermal listvenitization and associated mineralizations in Zagros Ophiolites: implications for mineral exploration in Iraqi Kurdistan. *J Geochem Explor* 208:106–404. <https://doi.org/10.1016/j.gexplo.2019.106404>
- Pirouei M, Kolo K, Kalaitzidis SP, Mustafa Abdullah S (2021) Newly discovered gossanite-like and sulfide ore bodies associated with microbial activity in the Zagros ophiolites from the Rayat area of NE Iraq. *Ore Geol Rev* 135:104–191. <https://doi.org/10.1016/j.oregeorev.2021.104191>
- Reimann C, de Caritat P (2017) Establishing geochemical background variation and threshold values for 59 elements in Australian surface soil. *Sci Total Environ* 578:633–648. <https://doi.org/10.1016/j.scitotenv.2016.11.010>
- Reimann C, Fabian K, Birke M et al (2018) GEMAS: establishing geochemical background and threshold for 53 chemical elements in European agricultural soil. *Appl Geochemistry* 88:302–318. <https://doi.org/10.1016/j.apgeochem.2017.01.021>
- Reimann C, Filzmoser P (2000) Normal and lognormal data distribution in geochemistry: death of a myth. Consequences for the statistical treatment of geochemical and environmental data. *Environ Geol* 39:1001–1014. <https://doi.org/10.1007/s002549900081>
- Reimann C, Filzmoser P, Garrett R, Dutter R (2008) *Statistical data analysis explained: applied environmental statistics with R*. In: *Statistical data analysis explained: applied environmental statistics with R*. Wiley, Chichester, pp 343
- Reimann C, Filzmoser P, Garrett RG (2005) Background and threshold: critical comparison of methods of determination. *Sci Total Environ* 346:1–16. <https://doi.org/10.1016/j.scitotenv.2004.11.023>
- Spadoni M (2006) Geochemical mapping using a geomorphologic approach based on catchments. *J Geochemical Explor* 90:183–196. <https://doi.org/10.1016/j.gexplo.2005.12.001>
- Tukey JW (1977) *Exploratory data analysis*, vol 688. Addison-Wesley, Reading, pp 581–582
- Vasiliev MM, Pentelikov VG (1962) Report on prospecting exploration of Bard-i-Zard chromite occurrence and adjacent areas in 1961. Report GEOSURV, Baghdad, Iraq
- Zheng Y, Sun X, Gao S et al (2014) Analysis of stream sediment data for exploring the Zhunuo porphyry Cu deposit, southern Tibet. *J Geochemical Explor* 143:19–30. <https://doi.org/10.1016/j.gexplo.2014.02.012>
- Zuo R (2011) Decomposing of mixed pattern of arsenic using fractal model in Gangdese belt, Tibet, China. *Appl Geochemistry* 26:S271–S273. <https://doi.org/10.1016/j.apgeochem.2011.03.122>